Available online at www.sciencedirect.com
ScienceDirect
Journal of Power Sources 172 (2007) 623–632
JOURNAL OF POWER SOURCES
www.elsevier.com/locate/jpowsour

# Effect of thermal annealing on the properties of $Co_{rich\ core}$–$Pt_{rich\ shell}$/C oxygen reduction electrocatalyst

Jing-Shan Do [a,*], Ya-Ting Chen [a], Mei-Hua Lee [a,b]

[a] *Nano Science and Technology Research Center and Department of Chemical Engineering, Tunghai University, Taichung 40704, Taiwan*
[b] *Department of Industrial Engineering and Management, Diwan College Management, Tainan 72141, Taiwan*

Received 2 March 2007; received in revised form 8 May 2007; accepted 12 May 2007
Available online 18 May 2007

**Abstract**

The properties and the oxygen reduction reaction (ORR) characteristics of Pt/C and $Co_{rich\ core}$–$Pt_{rich\ shell}$/C, which were prepared by the thermal decomposition and the chemical reduction methods, annealed in the various conditions were investigated. The alloying degree and grain size of $Co_{rich\ core}$–$Pt_{rich\ shell}$/C analyzed by XRD was increased from 13.10% and 2.45 nm to 42.83% and 2.62 nm by increasing the time for annealing at 400 °C in $N_2$ (annealing condition 1) from 0 to 15 h. When the $Co_{rich\ core}$–$Pt_{rich\ shell}$/C was annealed in air at 250 °C and then reduced in 6% $H_2$ at 400 °C (annealing condition 2), the alloying degree and grain size were obtained to be 47.26% and 3.79 nm, respectively. The decrease in the atomic ratio of Co/Pt from 4.77 to 1.34 by annealing $Co_{rich\ core}$–$Pt_{rich\ shell}$/C in condition 1 from 0 to 15 h was deduced to be the increase in the Pt loading by the reduction of residual Pt precursor to Pt. The mass and specific activities (MA, SA) of the ORR at 0.9 V (versus RHE) on Pt/C annealed in condition 2 were obtained to be 4.11 A $g^{-1}$ and 6.12 μA $cm^{-2}$, respectively. The MA and SA of $Co_{rich\ core}$–$Pt_{rich\ shell}$/C annealed by condition 2 were 10.07 A $g^{-1}$ and 11.27 μA $cm^{-2}$.


*Keywords:* PtCo electrocatalyst; Fuel cell; Oxygen reduction reaction; Thermal annealing; Electroactivity

## 1. Introduction

The chemical energy of fuel can be directly converted into the electrical energy by a fuel cell. The energy conversion efficiency is theoretically greater than that in a thermal cycle. The devices for treating the emissions may not be required due to the significant decrease in the pollutants from a fuel cell. In the polymeric electrolyte membrane fuel cell (PEMFC), the overpotential for the oxygen reduction reaction (ORR) on Pt electrocatalyst is about 0.2 V due to the strong bonding strength of $O_2$ and a high degree irreversibility of the reduction of $O_2$. This represents a loss 20% from the maximum theoretical energy efficiency of PEMFCs [1]. Platinum prepared on the carbon support exhibits the highest electrocatalytic activity of ORR by comparing with any of pure metals in the low temperature fuel cells [2]. In the recent years, platinum alloyed with various transition metals are employed to further improve the electrocatalytic activity of ORR and reduce the cost of electrocatalyst [3]. Many platinum alloys, such as PtCo, PtNi, PtFe, PtCr, have been prepared with various methods to use as the electrocatalysts of ORR [2,4–13].

The kinetics of ORR is much improved with Pt–Ni, Pt–Fe and Pt–Co prepared by sputtering method as cathodes due to the increase in d-electron vacancy of thin Pt surface layer caused by alloying [5]. When the atomic ratio of Pt–M (M = Co, Cr and Ni) is adjusted to 3:1, the lattice parameter of the Pt–M is smaller than Pt alone catalyst [7]. The ORR on Pt–M is demonstrated to be a structure-sensitive reaction. The mass activity (MA) of ORR on Pt–Cr alloy electrocatalyst is enhanced slightly, and the specific activity (SA) is much improved due to the change in lattice parameter and the surface composition by comparing with Pt alone electrocatalyst [11]. Furthermore, the Pt–Cr [11] and Pt–Ni [12] alloying electrocatalysts exhibit a higher methanol tolerance for the ORR than Pt/C electrocatalyst. Using Pt–M/C electrocatalysts prepared by the microemulsion method, the electroactivity ORR is greater than that of electrocatalysts prepared by the high-temperature route [13].

Recently, the synthesis and properties of the nanostructured core–shell materials have been investigated [14–35], and

* Corresponding author. Tel.: +886 4 23590262; fax: +886 4 23590009.
*E-mail address:* jsdo@thu.edu.tw (J.-S. Do).

0378-7753/$ – see front matter © 2007 Elsevier B.V. All rights reserved.
doi:10.1016/j.jpowsour.2007.05.020

the applications of the nanostructured core–shell materials are mainly focused on the magnetic materials, biomedicine and catalysts in the present date. Using $PtRu_5(CO)_{16}$ as the precursor, Pt is found preferentially at the core of PtRu nanoparticle treated at 473 K. An inverted structure is found for Pt appears mostly at the surface of the nanoparticle by treating at 673 K [14]. The $Co_{core}$–$Pt_{shell}$ nanoparticle prepared by the reaction of Co nanoparticle with $Pt(hfac)_2$ (hfac = hexafluoroacetylacetonate) is used as the magnetic material [17,18]. The catalytic characteristics of $Pd_{core}$–$Pt_{shell}$, which is synthesized by the successive addition method using sacrificial $H_2$, are investigated for the hydrogenation of methyl acrylate. The catalytic activity of Pd is enhanced by the presence of Pt [15]. The preparation of $Sn_{0.9}Si_{0.1}$/carbon core–shell nanoparticles and ZnO/CdSe nanowires are applied in the fields of lithium batteries [23] and solar cells [24], respectively. The bimetallic core–shell nanoparticles of Au–Ag, Au–Pd and Au–Pt are prepared and reported in the literatures [29–35]. However, the ORR on the core–shell type Pt–M (M = transition metal) electrocatalyst is seldom reported. The electrocatalytic activity for ORR may be enhanced by the presence of transition metal located within the core due to the structure and electronic effects caused by the partial alloying and vacant d-orbital from the transition metal, and the dissolution of the transition metal is expectably reduced due to the protection by Pt on the shell.

$Co_{rich\ core}$–$Pt_{rich\ shell}$ nanoparticle was prepared on carbon powder by the thermal decomposition and following by the chemical reduction, and used as the cathodic catalysts of ORR in this paper. The pristine electrocatalyst was annealed at various temperatures and environments. The properties and the electrochemical characteristics of Pt/C and $Co_{rich\ core}$–$Pt_{rich\ shell}$/C were also analyzed in this work.

## 2. Experimental

### 2.1. Preparation of Pt/C and $Co_{rich\ core}$–$Pt_{rich\ shell}$/C

Pt/C was prepared by the chemical reduction of platinum acetylacetonate ($Pt(acac)_2$) with 1,2-hexadecanediol as the reducing agent. The solution of 50 mg $Pt(acac)_2$, 100 mg 1,2-hexadecanediol, 56 μl oleic acid, 65 μl oleylamine dissolved in 10 ml diphenyl ether (dpe) mixed with 100 mg carbon powder (XC-72) was heated to 205 °C and refluxed in $N_2$ atmosphere for 1 h to prepare Pt/C (theoretical loading = 19.87%). A two-steps procedure was used to prepare $Co_{rich\ core}$–$Pt_{rich\ shell}$ nanoparticle on XC-72 carbon powder support. Firstly, 200 mg carbon powder was added into a solution of 60 mg dicobalt octacarbinyl ($Co_2(CO)_8$) dissolved in 10 ml dpe and heated to 142 °C and refluxed in $N_2$ atmosphere for 30 min. Then a solution of 50 mg $Pt(acac)_2$, 100 mg 1,2-hexadecanediol, 56 μl oleic acid, 65 μl oleylamine dissolved in 10 ml dpe was added and increased the refluxed temperature to 205 °C for 1 h. The obtaining $Co_{rich\ core}$–$Pt_{rich\ shell}$/C with the theoretical loading of 10.10% Pt and 8.43% Co was washed with ethyl alcohol for several times, and dried in a 100 °C vacuum oven for 24 h. Vulcan XC-72 was selected as the support of Pt and $Co_{rich\ core}$–$Pt_{rich\ shell}$ due to its high specific area of 250 $m^2\ g^{-1}$ and convenient comparison with the results in literatures.

The pristine $Co_{rich\ core}$–$Pt_{rich\ shell}$/C electrocatalyst was calcined at $N_2$ atmosphere in a tubular oven at various temperatures and holding times. The heat treatment of the pristine electrocatalyst was also taken place in air by increasing the temperature from the room temperature to 250 °C at a rate of 5 °C $min^{-1}$ and holding at 250 °C for 10 min. The metal oxides of electrocatalyst formed in the annealing process in air were reduced with 6% $H_2$/Ar in a tubular oven at 400 °C for 2 h.

The thermal properties of the pristine electrocatalysts were analyzed by a thermal gravimetric analyzer (TGA, TA Q50) in the $N_2$ and air environments, respectively. The crystallinities and particle sizes of the electrocatalysts were analyzed by the X-ray diffraction (XRD, Shimadzu XRD-6000) and the transmission electron microscope (TEM, JOEL JEM-1010), respectively. The electrocatalysts were firstly calcined at a 500 °C chamber furnace for 1 h to burn out the carbon support, and then dissolved in 12 ml aqua regia for analyzing its compositions with an atomic adsorption spectroscopy (AAS, Hitachi Z-6100).

### 2.2. Preparation of Pt/C/Au plate and $Co_{rich\ core}$–$Pt_{rich\ shell}$/C/Au plate electrodes for ORR

A suitable amount of electrocatalysts slurry prepared by mixing 10 mg $Co_{rich\ core}$–$Pt_{rich\ shell}$/C (or Pt/C) and a suitable amount of Nafion® solution (volume ratio of 5% Nafion® solution and DI water = 1/5) was cast on 1 $cm^2$ Au plate. The $Co_{rich\ core}$–$Pt_{rich\ shell}$/C/Au (or Pt/C/Au) was placed at room temperature and then at a 110 °C oven for drying. The electroactive area of electrocatalyst was measured by the cyclic voltammetry (CV) method with an electrochemical analyzer (CHI 611A) in 0.5 M $HClO_4$ aqueous solution in the absence of dissolved $O_2$ (sparging with $N_2$ for 30 min). The electrochemical characteristics of ORR on the pristine and annealed Pt/C/Au and $Co_{rich\ core}$–$Pt_{rich\ shell}$/C/Au electrocatalysts were carried out in the 0.5 M $HClO_4$ aqueous solution saturated with the dissolved $O_2$ by sparging $O_2$ for 30 min.

## 3. Results and discussion

### 3.1. Thermal gravimetric analysis (TGA) of electrocatalysts

#### 3.1.1. TGA of Co and Pt nanoparticles in $N_2$

As indicated in Section 2, the $Co_{rich\ core}$–$Pt_{rich\ shell}$/C was prepared by the thermal decomposition of $Co_2(CO)_8$ and then the reduction of $Pt(acac)_2$ in series. Hence some residual organic substances might exist on the surface of the pristine electrocatalysts. The thermal gravimetric curves of the nanoparticles of Co and Pt prepared by the thermal decomposition of $Co_2(CO)_8$ and the chemical reduction of $Pt(acac)_2$, respectively, were illustrated in Fig. 1. A slight decrease in the weight fraction found in Fig. 1a was inferred to be the evaporation of water (<280 °C) and dpe solvent from the Co nanoparticles. The weight fraction loss from 96% to 93% by increasing the temperature from 280 to 310 °C might be caused by the desorption of CO and $CO_2$,

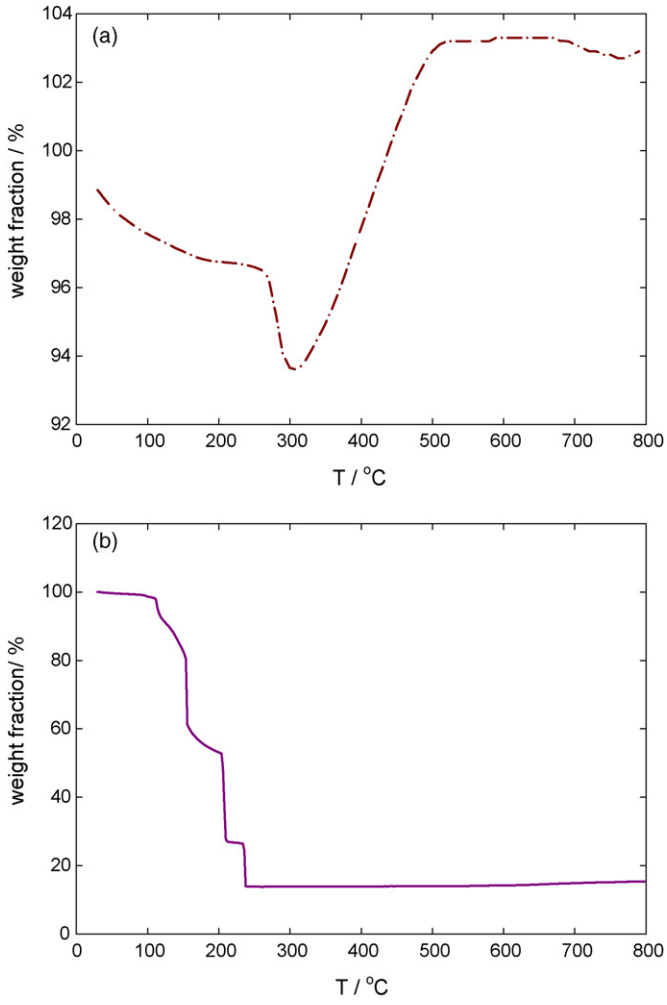


Fig. 1. TGA curves of (a) Co nanoparticle prepared by the thermal decomposition and (b) Pt nanoparticle produced by the chemical reduction. Purged gas: $N_2$, temperature raising rate = 20 °C min$^{-1}$, temperature range = 30–800 °C.

which were formed in the thermal decomposition of $Co_2(CO)_8$. The similar results were obtained for the TGA analysis of Co particle in the literature [36]. The oxidation of Co particle by the trace oxygen permeated from the environment into the TGA cell to form CoO and $Co_3O_4$ demonstrated by the XRD analysis resulted in the increase of the weight for the temperature greater than 310 °C. However, the slight variation of the weight fraction of Co particle prepared by the thermal decomposition of $Co_2(CO)_8$ in the TGA analysis revealed that the organic residuals remained on the Co nanoparticle were slight.

The TGA analysis of Pt nanoparticle obtained by the chemical reduction of $Pt(acac)_2$ indicated that the weight loss was 85% by increasing the temperature from 100 to 240 °C (Fig. 1b). The results revealed that a large amount of residuals, including the Pt precursor ($Pt(acac)_2$), surfactant and reductant, existed on the surface of Pt nanoparticles.

### 3.1.2. TGA of Co/C and $Co_{rich\ core}$–$Pt_{rich\ shell}$/C in air

The TGA curves of carbon support, Co/C and $Co_{rich\ core}$–$Pt_{rich\ shell}$/C illustrated in Fig. 2 indicated that the carbon was reacted with $O_2$ to $CO_2$ for temperature greater than 600 °C and

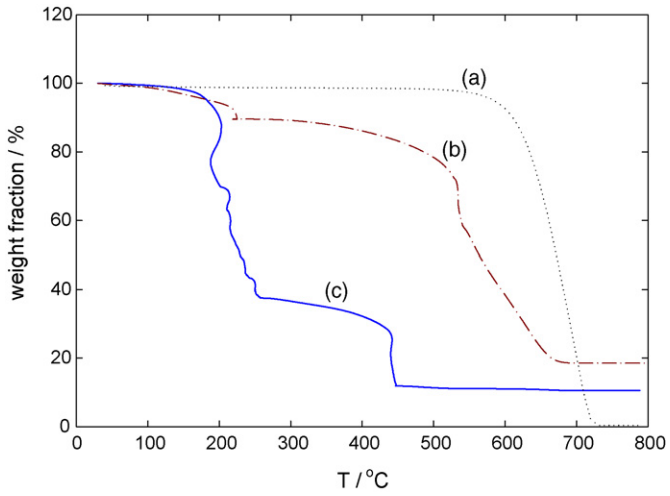


Fig. 2. TGA curves of (a) XC-72 carbon support, (b) as-prepared Co/C and (c) as-prepared $Co_{rich\ core}$–$Pt_{rich\ shell}$. Purged gas: air, temperature raising rate = 10 °C min$^{-1}$, temperature range = 30–800 °C.

resulted in the complete decomposition at 720 °C. The weight loss of 11% was found for Co/C at temperature less than 240 °C inferred to be the evaporation of adsorbed water and the residual organic solvent (dpe). The significant decrease in the weight fraction of Co/C for the temperature greater than 500 °C was caused by the decomposition of carbon support. The carbon support was completely decomposed at 680 °C, and a stable weight fraction was found to be 18.5% which was the cobalt oxides. The TGA curve of $Co_{rich\ core}$–$Pt_{rich\ shell}$/C revealed that the slight loss in weight for temperature less than 200 °C might be caused by the evaporation of the adsorbed water and the residual organic solvent, and the significant decrease in the weight fraction for temperature in the range of 200–250 °C was mainly due to the complex organics decomposition. The weight fraction loss at 450 °C was inferred to be the decomposition of carbon support. The experimental results revealed that the decomposition of carbon support was catalyzed by the presence of metal catalysts (Co and Pt) and resulted in the decrease of the decomposition temperature.

As the results in Fig. 2, the optimal temperature for removing the residual organics from $Co_{rich\ core}$–$Pt_{rich\ shell}$/C in air was 250 °C. The TGA of $Co_{rich\ core}$–$Pt_{rich\ shell}$/C annealed at 250 °C for various times in air are illustrated in Fig. 3. The similar TGA curves of $Co_{rich\ core}$–$Pt_{rich\ shell}$/C were found for the annealing time of 10, 30 and 60 min. The slight decrease in weight fraction for temperature less than 100 °C was caused by the evaporation of water adsorbed on the surface of electrocatalyst. For temperature in the range of 100–250 °C the insignificant decrease in the weight fraction of $Co_{rich\ core}$–$Pt_{rich\ shell}$/C annealed for various times revealed that the residual organics existed at the electrocatalyst were completely decomposed and removed by thermal annealing at 250 °C for 10 min.

### 3.2. The particle sizes of electrocatalysts

Using 1,2-hexadecanediol as reducing agent, Pt was deposited on carbon powder by the reduction of $Pt(acac)_2$. The

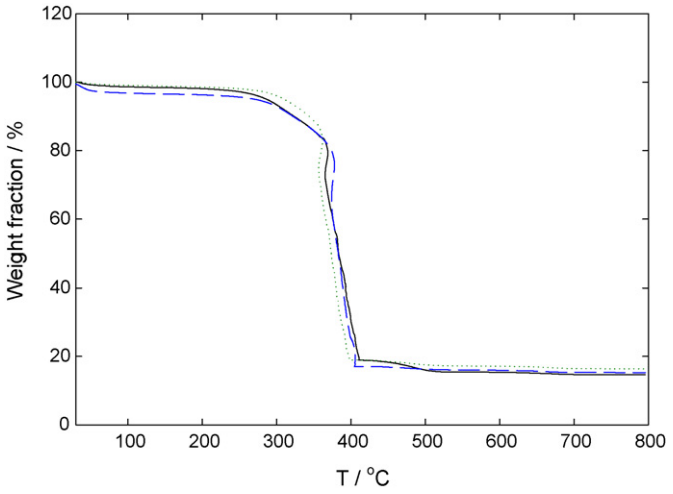


Fig. 3. TGA curves of $Co_{rich\ core}$–$Pt_{rich\ shell}$/C annealed at 250 °C in air. Purged gas: air, temperature raising rate = 10 °C $min^{-1}$, temperature range = 30–800 °C. Annealing time: (—) 10, (– – –) 30, (. . .) 60 min.

particle size of Pt on carbon powder was obtained to be 2–4 nm (Fig. 4a). The particle size of $Co_{rich\ core}$–$Pt_{rich\ shell}$/C prepared by the two-step procedure was illustrated in Fig. 4b and found to be 3–5 nm.

When the Pt/C was annealed at 400 °C in $N_2$ atmosphere for 5, 10 and 15 h, the particle sizes of Pt on C were found to be 2–4, 2–6 and 2–6 nm, respectively (Table 1). The slight growth of the Pt particle size was due to sintering in the thermal annealing process. Although, the Pt particle size was kept at the same range by increasing the annealing time from 10 to 15 h, the fraction of the larger Pt particle (6 nm) increased with the increase in the annealing time. The same particle size of $Co_{rich\ core}$–$Pt_{rich\ shell}$ on C was found for annealing at 400 °C in $N_2$ environment from 0 to 5 h (Table 1). Further increasing the annealing time to 10 and 15 h the particle size increased slightly to 3–6 nm. Similar to the results of Pt/C, the fraction of larger $Co_{rich\ core}$–$Pt_{rich\ shell}$ particle (i.e. 6 nm) on carbon support was also increased with the annealing time.

Table 1
Effect of thermal annealing on the particle size of Pt and $Co_{rich\ core}$–$Pt_{rich\ shell}$ on carbon support

| Thermal annealing[a] | Particle size (nm) | |
|---|---|---|
| | Pt | $Co_{rich\ core}$–$Pt_{rich\ shell}$ |
| – | 2–4 | 3–5 |
| Condition 1, 5 h | 2–4 | 3–5 |
| Condition 1, 10 h | 2–6 | 3–6 |
| Condition 1, 15 h | 2–6 | 3–6 |
| Condition 2 | 2–7 | 3–10 |

[a]Condition 1: The electrocatalyst was annealed at 400 °C in $N_2$. Condition 2: The electrocatalyst was annealed at 250 °C in air, and then reduced at 400 °C in 6% $H_2$ for 2 h.

The particle sizes of Pt and $Co_{rich\ core}$–$Pt_{rich\ shell}$ on C were obtained to be 2–7 and 3–10 nm, respectively, when the electrocatalysts were annealed at 250 °C in air and then reduced at 400 °C in 6% $H_2$ environment. Compared with the annealing in $N_2$ atmosphere the particle sizes of Pt and $Co_{rich\ core}$–$Pt_{rich\ shell}$ were significantly increased for annealing in air and reduction in 6% $H_2$ environment. The fraction of larger particle of Pt and $Co_{rich\ core}$–$Pt_{rich\ shell}$ on C annealed in air was significantly greater than that annealed in $N_2$, which were demonstrated in the TEM analysis.

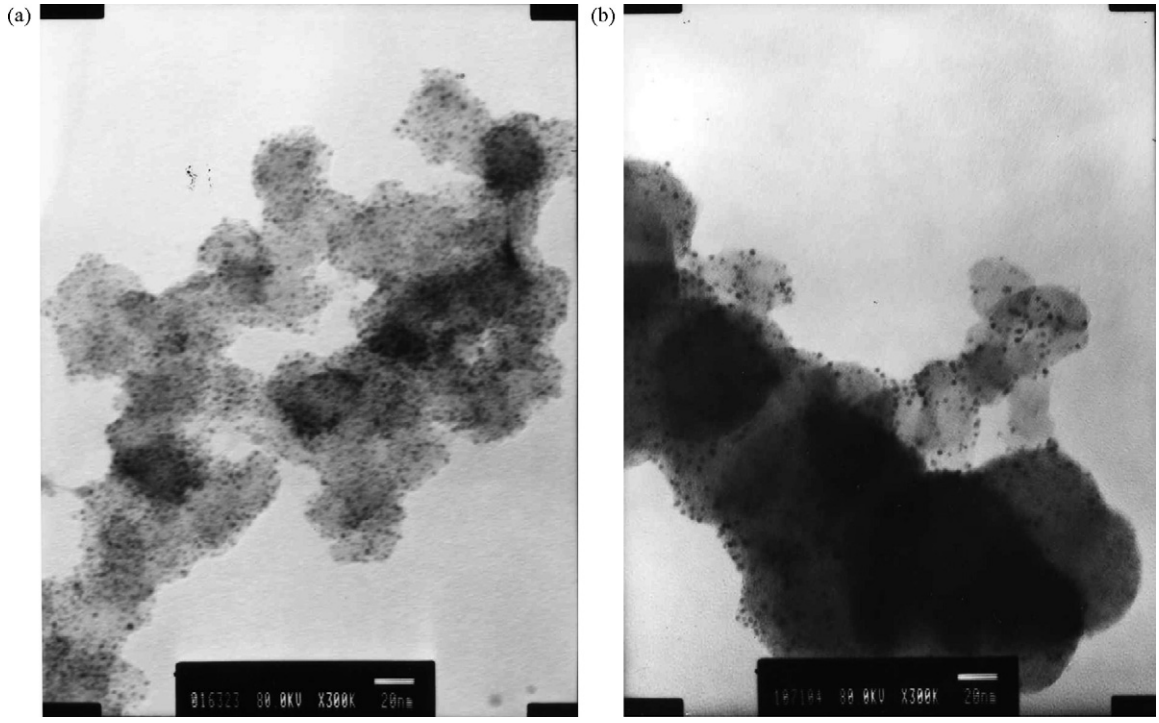


Fig. 4. TEM micrographs of pristine (a) Pt/C and (b) $Co_{rich\ core}$–$Pt_{rich\ shell}$/C.

### 3.3. Composition of electrocatalysts

The compositions of the pristine and thermal annealed electrocatalysts analyzed by AAS are shown in Table 2. The Pt loading of the pristine Pt/C (10.98%) less than the design value (19.87%) was due to uncompleted conversion of its precursor. In the thermal annealing procedure, the residual Pt precursor adsorbed on the pristine electrocatalyst was decomposed and reduced by the organic substances formed in the annealing procedure.

$$Pt(acac)_2 \xrightarrow[\Delta]{} Pt + CO_2 \uparrow + H_2O \uparrow \quad (1)$$

Therefore, the Pt loading of Pt/C increased from 11.68% to 14.79% when the time for annealing at 400 °C in $N_2$ was increased from 5 to 15 h (Table 2). At the same time, the conversion of Pt was increased from 58.78% to 74.43%. When the pristine Pt/C was annealed at air and then reduced in 6% $H_2$ environment, the similar results were obtained as indicated in Table 2. The increase in the loading and the conversion of Pt were mainly caused by the thermal decomposition of the Pt precursor and oxidization to be oxides, which was then reduced by $H_2$.

$$Pt(acac)_2 + O_2 \xrightarrow[\Delta]{} PtO + CO_2 \uparrow + H_2O \uparrow \quad (2)$$

$$PtO + H_2 \xrightarrow[\Delta]{} Pt + H_2O \uparrow \quad (3)$$

The loadings of Co and Pt on the pristine $Co_{rich\ core}$–$Pt_{rich\ shell}$/C were obtained to be 2.77% and 1.92% which were significantly less than their designed values of 8.43% and 10.10%. The lower loadings of Co and Pt might be caused by the low conversion of precursors ($Co_2(CO)_8$ and $Pt(acac)_2$), and a large amount of organic substances and the precursors absorbed on the carbon support. When the pristine $Co_{rich\ core}$–$Pt_{rich\ shell}$/C was annealed at 400 °C $N_2$ environment for 5 h, the weight loss of the electrocatalyst was found to be 31.55%, and the weight loss slightly increased to 36.00% for further increase in the annealing time to 15 h. The significant increase in the Co loading from 2.77% to 4.25% by increasing the annealing time from 0 to 5 h was inferred to be caused by the weight loss in the annealing procedure. The Co loading changed slightly for further increasing the annealing time to 15 h (Table 2; Fig. 5).

The Pt loading increased from 1.92% to 6.38% by increasing the annealing time from 0 to 5 h, and the Pt loading was increased to 10.16% by further increasing the annealing time to 15 h as illustrated in Table 2 and Fig. 5. The experimental results indicated that the increase in the Pt loading with the annealing time was significantly greater than that of the increase in Co loading for annealing at 400 °C in $N_2$ environment. The increase in the Pt loading in the annealing procedure was deduced to be caused by: (1) the weight loss of the electrocatalyst and (2) the decomposition and reduction of the Pt precursor adsorbed on the carbon support (Eq. (1)). Furthermore, the Pt precursor adsorbed on the carbon support might also be reduced by Co on $Co_{rich\ core}$–$Pt_{rich\ shell}$/C and caused the increase in the loading of Pt.

$$Pt(acac)_2 + Co \xrightarrow[\Delta]{} Pt + Co\ compounds \uparrow \quad (4)$$

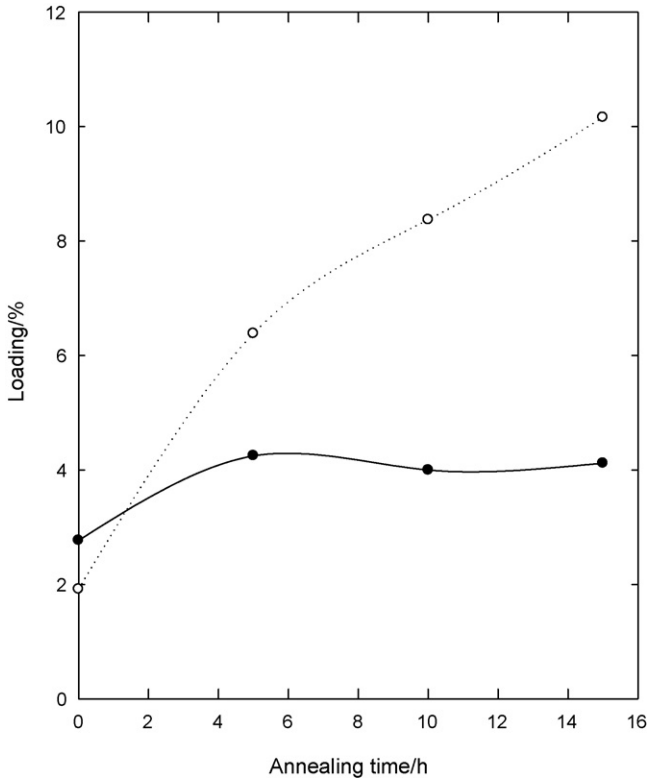


Fig. 5. Effect of annealing time in $N_2$ environment on the loadings of $Co_{rich\ core}$–$Pt_{rich\ shell}$/C. Conditions for preparing $Co_{rich\ core}$–$Pt_{rich\ shell}$/C: step 1: 200 mg XC-72, 60 mg $Co_2(CO)_8$ dissolved in 10 ml diphenyl ether, refluxed at 142 °C in $N_2$ for 30 min; step 2: 50 mg $Pt(acac)_2$, 100 mg 1,2-hexadecanediol, 56 μl oleic acid, 65 μl oleylamine dissolved in 10 ml dpe was added and increased the temperature to 205 °C refluxed for 1 h. Annealing temperature = 400 °C. Pt loading (◯), Co loading (●).

When the annealing time increased from 0 to 15 h in 400 °C $N_2$, the increase in the Pt loading was significantly greater than that of Co loading, and resulted in the decrease in the Co/Pt atomic ratio from 4.77 to 1.34 as shown in Table 2. When the pristine $Co_{rich\ core}$–$Pt_{rich\ shell}$/C was annealed in 250 °C air for 10 min and then reduced in 400 °C 6% $H_2$ for 2 h, the Co and Pt loadings increased to 4.24% and 6.19%, respectively. The less Pt loading for electrocatalyst annealed in air by comparing with the electrocatalyst annealed in $N_2$ was inferred to be the less annealing time and faster organic decomposition rate in air.

### 3.4. Crystallinity and alloying of electrocatalysts

The crystal faces of (1 1 1), (2 0 0), (2 2 0) and (3 1 1) were found in the XRD spectra of Pt/C, and the broad reflections indicated the nanostructured Pt with small grain sizes (Fig. 6). The grain size of Pt on the pristine Pt/C calculated based on the peak with $2\theta$ of 39.71° by using the Scherrer's equation [37] was 2.17 nm, which was correlated well with the particle size analyzed by TEM (Fig. 4a). Only the Pt peak of (1 1 1) was obvious for pristine $Co_{rich\ core}$–$Pt_{rich\ shell}$/C (Fig. 6), and the other peaks of Pt became unapparent. Compared with Pt/C the shift in peak angle of (1 1 1) from 39.71° to 40.31° was due to the intercalation of Co into the Pt fcc structure for $Co_{rich\ core}$–$Pt_{rich\ shell}$/C. The intercalation of Co into the Pt fcc

Table 2
Effect of the thermal annealing on the compositions of electrocatalysts

| Electrocatalysts | Annealing time (h)[a] | Loading (%) | | Conversion (%)[b] | | Atomic ratio of Co/Pt |
|---|---|---|---|---|---|---|
| | | Co | Pt | Co | Pt | |
| Pt/C | 0($N_2$) | – | 10.98 | – | 55.26 | – |
| | 5($N_2$) | – | 11.68 | – | 58.78 | – |
| | 10($N_2$) | – | 14.26 | – | 71.77 | – |
| | 15($N_2$) | – | 14.79 | – | 74.43 | – |
| | 1/6(air) | – | 14.50 | – | 72.97 | – |
| Co/C | 0($N_2$) | 13.0 | 88.58 | | – | |
| $Co_{rich\ core}$–$Pt_{rich\ shell}$/C | 0($N_2$) | 2.77 | 1.92 | 28.07 | 16.24 | 4.77 |
| | 5($N_2$) | 4.25 | 6.38 | 45.95 | 57.57 | 2.20 |
| | 10($N_2$) | 4.00 | 8.37 | 44.11 | 77.0 | 1.58 |
| | 15($N_2$) | 4.12 | 10.16 | 46.43 | 95.59 | 1.34 |
| | 1/6(air) | 4.24 | 6.19 | 45.75 | 55.72 | 2.26 |

[a] Thermal annealing in $N_2$ was set at 400 °C, and the thermal annealing in air was set at 250 °C for 10 min (1/6 h) and then reduced in 6% $H_2$ at 400 °C for 2 h.
[b] Conversion (%) = (moles of metal loading/moles of metal precursors) × 100%.

structure also caused the decrease in the lattice parameter from 0.391 (pristine Pt/C) to 0.387 (pristine $Co_{rich\ core}$–$Pt_{rich\ shell}$/C) nm (Table 3). Based on the results in the shift of diffraction angle and the change of the lattice parameter the alloying degree of the pristine $Co_{rich\ core}$–$Pt_{rich\ shell}$/C could be calculated based on Vegard's law [9] to be 13.10% (Table 3).

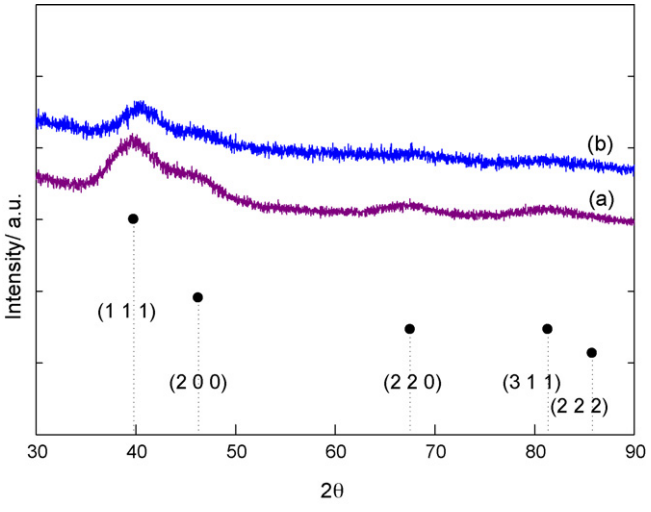


Fig. 6. XRD spectra of pristine (a) Pt/C and (b) $Co_{rich\ core}$–$Pt_{rich\ shell}$/C.

The grain size of Pt of Pt/C increased from 2.17 to 2.85 nm with the increase in the annealing time from 0 to 15 h at 400 °C in $N_2$ (Table 3). The grain size of Pt annealed in air and then reduced in 6% $H_2$ was obtained to be 4.40 nm, which was significantly greater than that annealed at $N_2$. As described in the above, the rate for decomposing residual organics adsorbed on the electrocatalysts in $N_2$ was less than that annealed in air. The growth of grain size by the thermal annealing in $N_2$ might hence be inhibited by the presence of residual organics on the electrocatalyst. On the other hand, the fast decomposition of residual organics for annealing in air resulted in the fast grain sintering and growth of grain size. The similar results were obtained for $Co_{rich\ core}$–$Pt_{rich\ shell}$/C as illustrated in Table 3. The atomic diffusion in the thermal annealing process led to the increase in the alloying degree and the decrease in the lattice parameter of $Co_{rich\ core}$–$Pt_{rich\ shell}$/C. When the $Co_{rich\ core}$–$Pt_{rich\ shell}$/C was annealed at 400 °C in $N_2$, the alloying degree increased from 13.10% to 42.83% and the lattice parameter decreased from 0.387 to 0.382 nm with the increase in the annealing time from 0 to 15 h (Table 3). The similar results were obtained

Table 3
Structure characteristics of eletrocatalysts

| Electrocatalysts | Annealing time (h)[a] | Pt | | Atomic ratio of Co/Pt | Alloying degree (%) |
|---|---|---|---|---|---|
| | | $GS^1$ (nm)[b] | $LP^2$ (nm)[b] | | |
| Pt/C | 0($N_2$) | 2.17 | 0.391 | – | – |
| | 5($N_2$) | 2.48 | 0.391 | – | – |
| | 10($N_2$) | 2.65 | 0.391 | – | – |
| | 15($N_2$) | 2.85 | 0.391 | – | – |
| | 1/6(air) | 4.40 | 0.391 | – | – |
| $Co_{rich\ core}$–$Pt_{rich\ shell}$/C | 0($N_2$) | 2.45 | 0.387 | 4.77 | 13.10 |
| | 5($N_2$) | 2.58 | 0.381 | 2.20 | 39.63 |
| | 10($N_2$) | 2.62 | 0.382 | 1.58 | 39.94 |
| | 15($N_2$) | 2.62 | 0.382 | 1.34 | 42.83 |
| | 1/6(air) | 3.79 | 0.379 | 2.26 | 47.26 |

[a] Thermal annealing in $N_2$ was set at 400 °C, and the thermal annealing in air was set at 250 °C for 10 min (1/6 h) and then reduced in 6% $H_2$ at 400 °C for 2 h.
[b] 1: GS, grain size; 2: LP, lattice parameter.

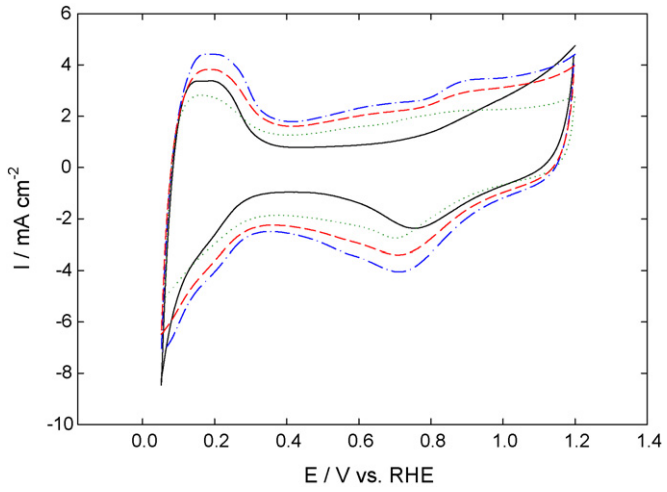


Fig. 7. Cyclic voltammograms of Pt/C annealed at 400 °C in $N_2$ for various times. WE: Pt/C annealed at 400 °C in $N_2$, geometric area of WE = 1 $cm^2$, RE: RHE (0.5 M $HClO_4$), CE: Pt foil, electrolyte: 0.5 M $HClO_4$, room temp., scan rate = 50 mV $s^{-1}$, scan range = 0.05–1.2 V. Conditions for preparing Pt/C: 100 mg XC-72, 50 mg $Pt(acac)_2$, 100 mg 1,2-hexadecanediol, 56 μl oleic acid, 65 μl oleylamine dissolved in 10 ml diphenyl ether, temp. = 205 °C, refluxed in $N_2$ atmosphere for 1 h. Annealing time: (—) 0, (– – –) 5, (– · –) 10, (. . .) 15 h.

for the $Co_{rich\ core}$–$Pt_{rich\ shell}$/C annealed in air and reduced in 6% $H_2$.

### 3.5. Electrochemical measurement

#### 3.5.1. Electroactive area

The cathodic reduction of $H^+$ in 0.5 M $HClO_4$ aqueous solution on Pt/C was found for the potential less than 0.4 V (versus RHE), and the adsorbed hydrogen was oxidized for the reverse scanning from 0.05 V (RHE) as illustrated in the cyclic voltammograms (Fig. 7). The similar cyclic voltammograms were obtained on Pt/C annealed at 400 °C in $N_2$ for various times. The electroactive area of Pt calculated from the charges for the oxidation of the adsorbed hydrogen on the Pt surface increased from 49.53 to 55.81 $m^2\ g^{-1}$ by increasing the annealing time from 0 to 5 h (Table 4). The decomposition and remove of the residual organics from the Pt surface resulted in the increase of the electroactive area. Further increasing the annealing time to 15 h, the electrochemical area decreased to 37.87 $m^2\ g^{-1}$ due to the growth of the Pt grain in the thermal annealing process (Table 4).

The maximum electroactive area of Pt on $Co_{rich\ core}$–$Pt_{rich\ shell}$/C without thermal annealing obtained to be 117.69 $m^2\ g^{-1}$ was inferred to be the relative lower Pt loading and the sufficient dispersion of Pt on the Co/C, which was caused by the higher atomic ratio of Co/Pt (4.77). The significant increase in the Pt loading of $Co_{rich\ core}$–$Pt_{rich\ shell}$/C by increasing the annealing time resulted in the decrease in the atomic ratio of Co/Pt (Table 2). When the time for annealing $Co_{rich\ core}$–$Pt_{rich\ shell}$/C at 400 °C in $N_2$ increased from 0 to 15 h, the electroactive area of Pt hence decreased from 117.69 to 51.98 $m^2\ g^{-1}$ caused by the decrease in the dispersive degree of Pt. The electroactive area of Pt on Pt/C and $Co_{rich\ core}$–$Pt_{rich\ shell}$/C were evaluated to be 73.61 and 89.29 $m^2\ g^{-1}$, respectively, for the electrocatalysts annealed in air and reduced in 6% $H_2$. Compared with the electrocatalysts annealed in air the less electroactive area of Pt on the electrocatalysts annealed in $N_2$ might be due to the uncompleted decomposition and remove of the residual organics from the electrocatalysts.

Table 4
Effect of annealing time on the electroactive area of Pt

| Electrocatalysts | Annealing time (h)[a] | Electroactive area ($m^2\ g^{-1}$) |
|---|---|---|
| Pt/C | 0($N_2$) | 49.53 |
| | 5($N_2$) | 55.81 |
| | 10($N_2$) | 46.39 |
| | 15($N_2$) | 37.87 |
| | 1/6(air) | 73.61 |
| $Co_{rich\ core}$–$Pt_{rich\ shell}$(1:1)/C | 0($N_2$) | 117.69 |
| | 5($N_2$) | 60.15 |
| | 10($N_2$) | 58.84 |
| | 15($N_2$) | 51.98 |
| | 1/6(air) | 89.29 |
| $Co_{rich\ core}$–$Pt_{rich\ shell}$(1:2)/C | 0($N_2$) | 56.76 |
| | 1/6(air) | 96.69 |

[a] Thermal annealing in $N_2$ was set at 400 °C, and the thermal annealing in air was set at 250 °C for 10 min (1/6 h) and then reduced in 6% $H_2$ at 400 °C for 2 h.

#### 3.5.2. Oxygen reduction reaction

Changing the scanning rate of linear sweep from 1.0 to 0.2 mV $s^{-1}$ in 0.5 M $HClO_4$ aqueous solution on the pristine Pt/C a steady current and potential relationship (*I–E* curve) were obtained for the scanning rate less than 0.5 mV $s^{-1}$. Using Pt/C annealed in $N_2$ with the various times as the cathodes, the cathodic reduction of oxygen was found for the potential less than 1.0 V (versus RHE), and the ORR was controlled by the electrochemical kinetics for the potential in the range of 1.0–0.9 V as indicated in Fig. 8. When the potential of cathode was less than 0.8 V, the ORR was controlled by the mass transfer of dissolved oxygen from the bulk solution to the surface of electrocatalyst. The relative lower electroactive area of Pt/C annealed in $N_2$ for 15 h (37.87 $m^2\ g^{-1}$ as shown in Table 4) resulted in the least limiting current density of ORR by comparing with the other Pt/C (Fig. 8).

The similar currents of ORR on Pt/C annealed in $N_2$ for various times were obtained at the same applied potential in the kinetic controlled region, i.e. potential greater than 0.9 V versus RHE. However, the loading of Pt on the Pt/C annealed in $N_2$ increased and the electroactive area decreased by increasing the annealing time as illustrated in Tables 2 and 4. Therefore, the mass activity (MA) of ORR decreased from 3.07 to 1.95 A $g^{-1}$ at 0.9 V (versus RHE) with the increase in the annealing time from 0 to 15 h (Table 5). Increasing the annealing time in $N_2$ from 0 to 10 h the specific activity (SA) of ORR decreased from 5.53 to a minimum value of 4.85 μA $cm^{-2}$. Further increasing the annealing time to 15 h the SA was increased to 5.40 μA $cm^{-2}$ (Table 5). As indicated in Fig. 9, the structure and the relative strength of the various crystal faces changed with the thermal

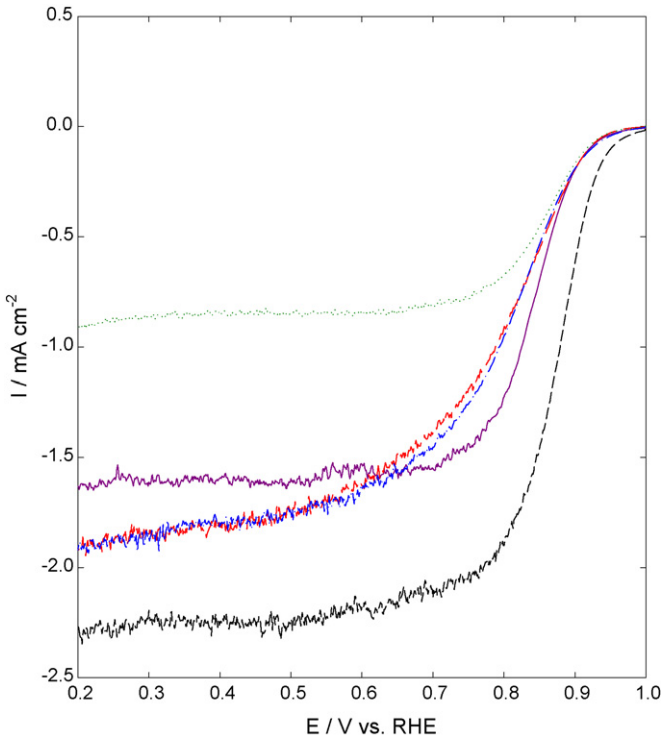


Fig. 8. Linear scan voltammograms of ORR on Pt/C. WE: Pt/C, geometric area of WE = 1 $cm^{-2}$, RE: RHE (0.5 M $HClO_4$), CE: Pt foil, electrolyte: 0.5 M $HClO_4$ with $O_2$-saturated, room temp., scan rate: 0.5 mV $s^{-1}$, $O_2$ flow rate = 40 ml $min^{-1}$, agitation rate = 200 rpm. Conditions for preparing Pt/C: 100 mg XC-72, 50 mg $Pt(acac)_2$, 100 mg 1,2-hexadecanediol, 56 μl oleic acid, 65 μl oleylamine dissolved in 10 ml diphenyl ether, temp. = 205 °C, refluxed in $N_2$ atmosphere for 1 h. Time for annealing at 400 °C in $N_2$: (—) 0, (– – –) 5, ( – · – ) 10, (. . .) 15 h. (– – – –) Annealing at 250 °C in air for 10 min and reducing at 400 °C in 6% $H_2$ for 2 h.

annealing time. In general the ORR on Pt was demonstrated to be a structure-sensitive reaction [38,39]. Therefore, the change of SA of ORR on Pt/C with the annealing time in $N_2$ was inferred to be the change of the structure and the grain size of Pt on the carbon support. Compared with the Pt/C annealed in $N_2$

Table 5
Effect of annealing time on the electrochemical activities of electrocatalysts

| Electrocatalysts | Annealing time (h)[a] | MA[1]/A ($g^{-1}$)[b] | SA[2] (μA $cm^{-2}$)[b] |
|---|---|---|---|
| Pt/C | 0($N_2$) | 3.07 | 5.53 |
| | 5($N_2$) | 2.84 | 5.10 |
| | 10($N_2$) | 2.24 | 4.85 |
| | 15($N_2$) | 1.95 | 5.40 |
| | 1/6(air) | 4.11 | 6.12 |
| $Co_{rich\ core}$–$Pt_{rich\ shell}$(1:1)/C | 0($N_2$) | 10.45 | 8.26 |
| | 5($N_2$) | 4.79 | 8.00 |
| | 10($N_2$) | 5.48 | 8.80 |
| | 15($N_2$) | 6.21 | 12.02 |
| | 1/6(air) | 10.07 | 11.27 |

[a] Thermal annealing in $N_2$ was set at 400 °C, and the thermal annealing in air was set at 250 °C for 10 min (1/6 h) and then reduced in 6% $H_2$ at 400 °C for 2 h.

[b] 1: Mass activity was measured based on the potential of 0.9 V (vs. RHE). 2: Specific activity was measured based on the potential of 0.9 V (vs. RHE).

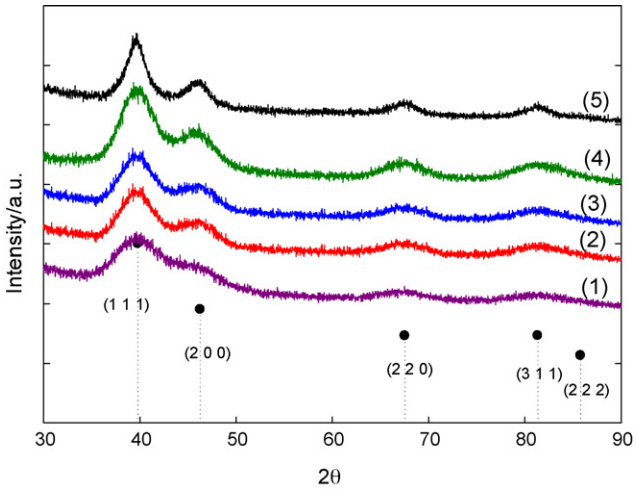


Fig. 9. XRD spectra of Pt/C. Conditions for preparing Pt/C: 100 mg XC-72, 50 mg $Pt(acac)_2$, 100 mg 1,2-hexadecanediol, 56 μl oleic acid, 65 μl oleylamine dissolved in 10 ml diphenyl ether, temp. = 205 °C, refluxed in $N_2$ atmosphere for 1 h. Time for annealing at 400 °C in $N_2$: (1) 0, (2) 5, (3) 10, (4) 15 h; (5) annealing at 250 °C in air for 10 min and reducing at 400 °C in 6% $H_2$ for 2 h.

the significant larger MA and SA of ORR on Pt/C annealed in air was mainly attributed to the elimination of organic residuals more completely, the change in the crystal structure (Fig. 9) and shifting the *I–E* curve to a direction of positive potential.

Similar electrochemical behaviors of ORR were found for using $Co_{rich\ core}$–$Pt_{rich\ shell}$/C annealed in $N_2$ with the various times as cathodes (Fig. 10). The oxygen was reduced at potential less than 1.0 V (versus RHE) and the limiting current of ORR was found for the potential less than 0.8 V. The least limiting current of ORR obtained on $Co_{rich\ core}$–$Pt_{rich\ shell}$/C without thermal annealing was mainly due to the least Pt loading (1.92% as shown in Table 2) and large amount of organic residuals adsorbed on the electrocatalyst. The significant increase in the Pt loading (Table 2) resulted in the increase in the limiting current of ORR with the increase in the annealing time in $N_2$ (Fig. 10). The maximum MA obtained to be 10.45 A $g^{-1}$ based on $Co_{rich\ core}$–$Pt_{rich\ shell}$/C without thermal annealing was attributed to the maximum electroactive area of 117.69 $m^2$ $g^{-1}$ (Table 4). The least Pt loading of $Co_{rich\ core}$–$Pt_{rich\ shell}$/C without thermal annealing resulted in the higher dispersion of Pt on Co/C and the maximum electroactive area. The increase in SA of ORR on $Co_{rich\ core}$–$Pt_{rich\ shell}$/C from 8.26 to 12.02 μA $cm^{-2}$ with the annealing time from 0 to 15 h might be due to the increase in the alloying degree and the decrease in the lattice parameter (Table 3). Furthermore, increasing the alloying degree the fraction of Co present at the surface of electrocatalyst increased and the stable state of the alloying metal (Co) was most likely in an "oxidized state" attached with one or more OH ligands [40]. The presence of OH on Co could prevent the adsorption of OH on the neighboring Pt and increased the ORR activity. When $Co_{rich\ core}$–$Pt_{rich\ shell}$/C was annealed in air, the higher values of MA (10.07 A $g^{-1}$) and SA (11.27 μA $cm^{-2}$) of ORR were deduced to be the higher electroactive area (89.26 $m^2$ $g^{-1}$) and alloying degree (47.26%).

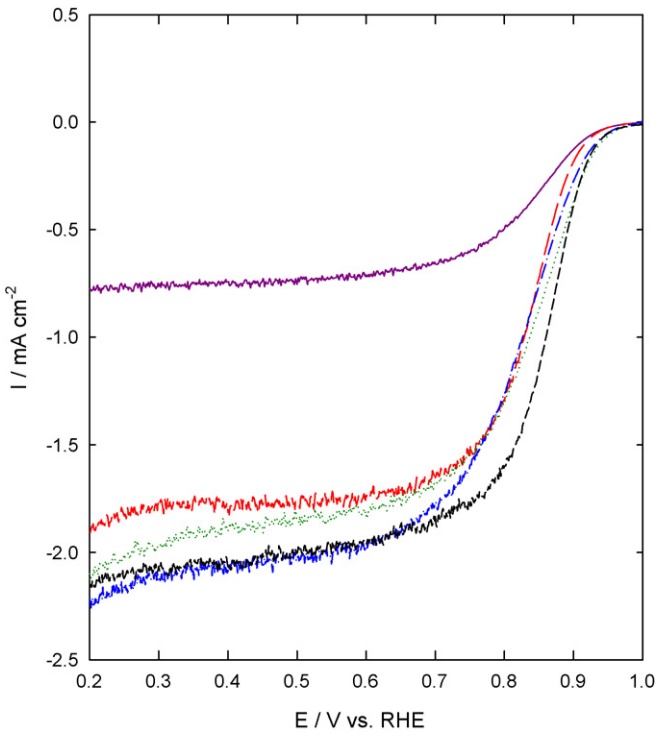


Fig. 10. Linear scan voltammograms of ORR on $Co_{rich\ core}$–$Pt_{rich\ shell}$/C. WE: $Co_{rich\ core}$–$Pt_{rich\ shell}$/C, geometric area of WE = 1 $cm^2$; RE: RHE (0.5 M $HClO_4$), CE: Pt foil, electrolyte: 0.5 M $HClO_4$ with $O_2$-saturated, room temp., scan rate: 0.5 mV $s^{-1}$, $O_2$ flow rate: 40 ml $min^{-1}$, agitation rate: 200 rpm. Conditions for preparing $Co_{rich\ core}$–$Pt_{rich\ shell}$/C: step 1: 200 mg XC-72, 60 mg $Co_2(CO)_8$ dissolved in 10 ml diphenyl ether, refluxed at 142 °C in $N_2$ for 30 min; step 2: 50 mg $Pt(acac)_2$, 100 mg 1,2-hexadecanediol, 56 μl oleic acid, 65 μl oleylamine dissolved in 10 ml dpe was added and increased the temperature to 205 °C refluxed for 1 h.

In general the MA and SA of ORR based on $Co_{rich\ core}$–$Pt_{rich\ shell}$/C were greater than that on Pt/C. The higher MA of ORR revealed that a greater part of Pt on $Co_{rich\ core}$–$Pt_{rich\ shell}$/C was located on the surface of electrocatalyst and hence the Pt utility of $Co_{rich\ core}$–$Pt_{rich\ shell}$/C was greater than that of Pt/C. The decrease in the lattice parameter and the adsorption of OH on Pt was due to the presence of Co on $Co_{rich\ core}$–$Pt_{rich\ shell}$/C. Therefore, the SA of ORR on $Co_{rich\ core}$–$Pt_{rich\ shell}$/C was greater than that on Pt/C.

## 4. Conclusions

Platinum was prepared on the carbon support by the chemical reduction, and the part of $Pt(acac)_2$ were decomposed and reduced to be Pt in the thermal annealing processes. The Pt loading increased from 10.98% to 14.50% by increasing the annealing time in $N_2$ from 0 to 15 h. $Co_{rich\ core}$–$Pt_{rich\ shell}$/C was prepared by the thermal decomposition of $Co_2(CO)_8$ and the chemical reduction of $Pt(acac)_2$ in series. Increasing the time of thermal annealing in $N_2$ from 0 to 15 h the decomposition and reduction of residual Pt precursor on $Co_{rich\ core}$–$Pt_{rich\ shell}$/C resulted in the increase in the Pt loading from 1.92% to 10.16%, the decrease in the Co/Pt atomic ratio from 4.77 to 1.34. The alloying degree of $Co_{rich\ core}$–$Pt_{rich\ shell}$/C was increased from 13.10% to 42.83% with the increase in the annealing time in $N_2$ from 0 to 15 h. The maximum Pt electroactive area of 117.69 $m^2\ g^{-1}$ for the pristine $Co_{rich\ core}$–$Pt_{rich\ shell}$/C was attributed by the higher dispersion of Pt on Co nanoparticle and carbon support. Compared with the annealed in $N_2$ the higher electroactive area of electrocatalysts annealed in air was deduced to the complete decomposition of residual organics adsorbed on the electrocatalysts. The MA and SA of ORR on Pt/C annealed in air were higher than that annealed in $N_2$ due to the higher electroactive area and change in the crystal structure of Pt. The increase in the SA of ORR on $Co_{rich\ core}$–$Pt_{rich\ shell}$/C annealed in $N_2$ from 8.22 to 12.02 with the increase in annealing time from 0 to 15 h was mainly caused by the increase in the alloying degree. The $Co_{rich\ core}$–$Pt_{rich\ shell}$/C electrocatalyst annealed in air exhibited the higher MA and SA of ORR, which were 10.07 A $g^{-1}$ and 11.27 μA $cm^{-2}$, were 2.45- and 1.84-folds of Pt/C annealed in air.

## Acknowledgements

The financial support of National Science Council of the Republic of China (Project number: NSC-94-2120-M-011-002) and Tunghai University is acknowledged.

## References

[1] A.S. Arico, A.K. Shukla, H. Kim, S. Park, M. Min, V. Antonucci, Appl. Surf. Sci. 172 (2001) 33.
[2] E. Antolini, Mater. Chem. Phys. 78 (2003) 563.
[3] P. Yu, M. Pemberton, P. Plasse, J. Power Sources 144 (2005) 11.
[4] V. Mehta, J.S. Cooper, J. Power Sources 114 (2003) 32.
[5] T. Toda, H. Igarashi, H. Uchida, M. Watanabe, J. Electrochem. Soc. 146 (1999) 3750.
[6] J. Shim, D.-Y. Yoo, J.S. Lee, Electrochim. Acta 45 (2000) 1943.
[7] M.-K. Min, J. Cho, K. Cho, H. Kim, Electrochim. Acta 45 (2000) 4211.
[8] M. Neergat, A.K. Shukla, K.S. Gandhi, J. Appl. Electrochem. 31 (2001) 373.
[9] J.R.C. Salgado, E. Antolini, E.R. Gonzalez, J. Power Sources 138 (2004) 56.
[10] W. Li, W. Zhou, H. Li, Z. Zhou, B. Zhou, Electrochim. Acta 49 (2004) 1045.
[11] H. Yang, N. Alonso-Vante, J.-M. Leger, C. Lamy, J. Phys. Chem. B 108 (2004) 1938.
[12] H. Yang, C. Coutanceau, J.-M. Leger, A.-V. Nicolas, C. Lamy, J. Electroanal. Chem. 576 (2005) 305.
[13] L. Xiong, A. Manthiram, Electrochim. Acta 50 (2005) 2323.
[14] M.S. Nasjner, A.I. Frenkel, D. Somerville, C.W. Hills, J.R. Shapley, R.G. Nuzzo, J. Am. Chem. Soc. 120 (1998) 8093.
[15] N. Toshima, Y. Shiraishi, A. Shiotsuki, D. Ikenaga, Y. Wang, Eur. Phys. J. D 16 (2001) 209.
[16] J. Lin, W. Zhou, A. Kumbha, J. Wiemann, J. Fang, E.E. Carpenter, C.J. O'Connor, J. Solid State Chem. 159 (2001) 26.
[17] J.-I. Park, J. Cheon, J. Am. Chem. Soc. 123 (2001) 5743.
[18] J.-I. Park, M.G. Kim, Y.-W. Jun, J.-S. Lee, J. Cheon, J. Am. Chem. Soc. 126 (2004) 9072.
[19] N.S. Sobal, M. Hilgendorff, H. Möhwald, M. Giersig, Nano Lett. 2 (2002) 621.
[20] X. Teng, H. Yang, J. Am. Chem. Soc. 125 (2003) 14559.
[21] N.S. Sobal, U. Ebels, H. Möhwald, M. Giersig, J. Phys. Chem. B 107 (2003) 7351.
[22] S. Xu, B. Zhao, W. Xu, Y. Fan, Colloids Surf. A Physicochem. Eng. Aspects 257/258 (2005) 313.
[23] Y. Kwon, H. Kim, S.-G. Doo, J. Cho, Chem. Mater. 19 (2007) 982.

[24] R. Tena-Zaera, A. Katty, S. Bastide, C. Lévy-Clément, Chem. Mater. 19 (2007) 1626.
[25] M. Agrawal, A. Pich, N.E. Zafeiropoulos, S. Gupta, J. Pionteck, F. Simon, M. Stamm, Chem. Mater. 19 (2007) 1845.
[26] B.E. Solsona, J.K. Edwards, P. Landon, A.F. Carley, A. Herzing, C.J. Kiely, G.J. Hutchings, Chem. Mater. 18 (2006) 2689.
[27] S. Shanmugam, A. Gabashvili, D.S. Jacob, J.C. Yu, A. Gedanken, Chem. Mater. 18 (2006) 2275.
[28] J.-S. Jan, S. Lee, C.S. Carr, D.F. Shantz, Chem. Mater. 17 (2005) 4310.
[29] I. Srnova-Sloufova, B. Vlckova, Z. Bastl, T.L. Hasslett, Langmuir 20 (2004) 3407.
[30] T. Shibata, B.A. Bunker, Z. Zhang, D. Meisel, C.F.I.I. Vardeman, J.D. Gezelter, J. Am. Chem. Soc. 124 (2002) 11989.
[31] N. Toshima, M. Harada, Y. Yamazaki, K. Asakura, J. Phys. Chem. 96 (1992) 9927.
[32] Y. Mizukoshi, K. Okitsu, Y. Maeda, T.A. Zamamoto, R. Oshima, Y. Nagata, J. Phys. Chem. B 101 (1997) 7033.
[33] G. Schmid, A. Lehnert, J.O. Malm, J.O. Bovin, Angew. Chem. Int. Ed. Engl. 30 (1991) 874.
[34] F. Mafuné, J. Kohno, Y. Takeda, T. Kondow, J. Am. Chem. Soc. 125 (2003) 1686.
[35] L. Qian, X. Yang, Colloids Surf. A: Physicochem. Eng. Aspects 260 (2005) 79.
[36] D.N. Srivastava, V.G. Pol, O. Palchik, L. Zhang, J.C. Yu, A. Gedanken, Ultrason. Sonochem. 12 (2005) 205.
[37] A.R. West, Solid State Chemistry and its Applications, Wiley, New York, 1984.
[38] B.N. Grgur, N.M. Markovic, P.N. Ross, Can. J. Chem. 75 (1997) 1465.
[39] M. Markovic, H. Gasteiger, P.N. Ross, J. Electrochem. Soc. 144 (1997) 1591.
[40] U.A. Palus, A. Wokaun, G.G. Scherer, T.J. Schmidt, V. Stamenkovic, N.M. Markovic, P.N. Ross, Electrochim. Acta 47 (2002) 3787.